

Femtosecond-Laser-Ablated Porous Silver Nanowire Heater with Ultralow Driven-Voltage and Ultrafast Sensitivity for Highly Efficient Crude Oil Remedy

Youdi Hu,[†] Chao Chen,[†] Chaowei Wang,* Qing-Fang Guan, Yanlei Hu, Jincheng Ni, Dong Wu,* and Shu-Hong Yu



Cite This: *Nano Lett.* 2025, 25, 1520–1527



Read Online

ACCESS |



Metrics & More



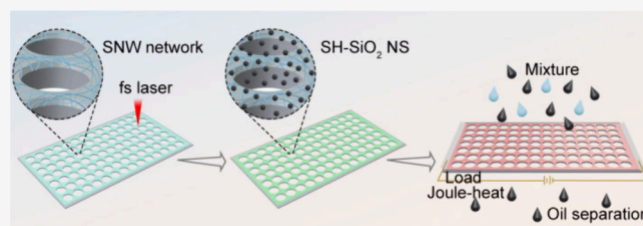
Article Recommendations



Supporting Information

ABSTRACT: The development of viscous-crude oil and water separation technology is important for overcoming pollution caused by oil spills. Although some separators responding to light, electric, and temperature have been proposed, their poor structural homogeneity and inferior controllability, together with weak capillary forces, hinder the rapid salvage of viscous crude oil. Herein, a Joule-heated hydrophobic porous oil/water separator is reported, which has advantages of low energy consumption ($169.7 \text{ }^\circ\text{C}\cdot\text{cm}^2\cdot\text{W}^{-1}$), short thermal-response time (5 s) and rapid heating rate ($13 \text{ }^\circ\text{C}/\text{s}$). Under an ultralow voltage of 4.5 V, crude oil could infiltrate through the separator within 5 s. COMSOL simulation reveals the thermodynamics of crude oil's unidirectional collection. Significantly, the gradient wettability originating from the asymmetrical temperature on the dual face is the dominant driving force for efficient oil/water separation. Finally, a homemade device is successfully deployed for continuous viscous oil/water separation. This work provides a new avenue for viscous oil remedy.

KEYWORDS: viscous oil/water separation, femtosecond laser processing, silver nanowire film, Joule-heated effect, low energy consumption



With the increasing occasion of oil spills, severe water pollution has been induced and therefore aroused great attention owing to its potential hazards in human activities and the environment. To purify the water/oil mixture,^{1–6} people have paved great efforts to develop a diversity of separators based on graphene sponges,^{7–9} carbon nanotube gels,^{10,11} and two-dimensional material films.^{12–14} Unfortunately, the above materials and membranes present lower separating efficiency, especially for the remedy of heavy crude oil. Considering that the heavy crude oil exhibits a high viscosity ranging from 10^3 to 10^5 mPa·s, the separator would be easily blocked during the separating process, resulting in its deterioration and even failure. In this regard, the recovery of heavy crude oil featuring an exaggerated viscous force is still challenging.

As is known, the viscosity of oil tends to decrease sharply with the elevation of its surrounding temperature, which could be easily detected from our daily cooking process. Inspired by the above phenomenon, Yu and his co-workers pioneeringly put forward a new paradigm of Joule-heating separator, which is made of graphene-married porous sponge.¹⁵ Once tens of voltages are applied on this separator, the generated Joule-heat is able to actuate a sharp decrease of the oil viscosity from 10^5 to 10^1 mPa·s, thereby realizing the continuous remedy of heavy crude oil. Notably, the unparalleled advantage of this strategy is that the Joule-heating separator can accelerate the salvage of heavy crude oil and would not be blocked.

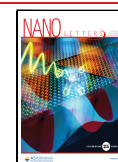
Following this classical method, a lot of calorific separators springs up on the basis of Joule-heating effect^{16,17} as well as photothermal effect.^{18–22} For example, Zhang proposed the solar-driven self-heating hydrophobic/oleophilic sponges, achieving crude oil from water surfaces.¹⁸ Li developed a *Crassula perforata*-structured CuO@CuS/PDMS nanowire arrays with effective light-to-heat conversion to clean up viscous crude oil;¹⁹ Kuang reported a solar-heated carbon absorber for the rapid cleanup of viscous oil spills.²⁰ Overall, most previously explored separators have two crucial components including the electrical/photoresponsive functional material and a hydrophobic porous skeleton.^{23–25} Though these separators have advanced the effective remedy of heavy crude oil from water, several drawbacks arise subsequently: (i) graphene or other carbon materials are often actuated by several hundred voltages attributed to their higher electrical resistance, resulting in extensive energy consumption. (ii) Although the photothermal separators are energy-saving, they would not work in cloudy climates with poor illumination. (iii) Most hydrophobic

Received: November 2, 2024

Revised: January 9, 2025

Accepted: January 13, 2025

Published: January 15, 2025



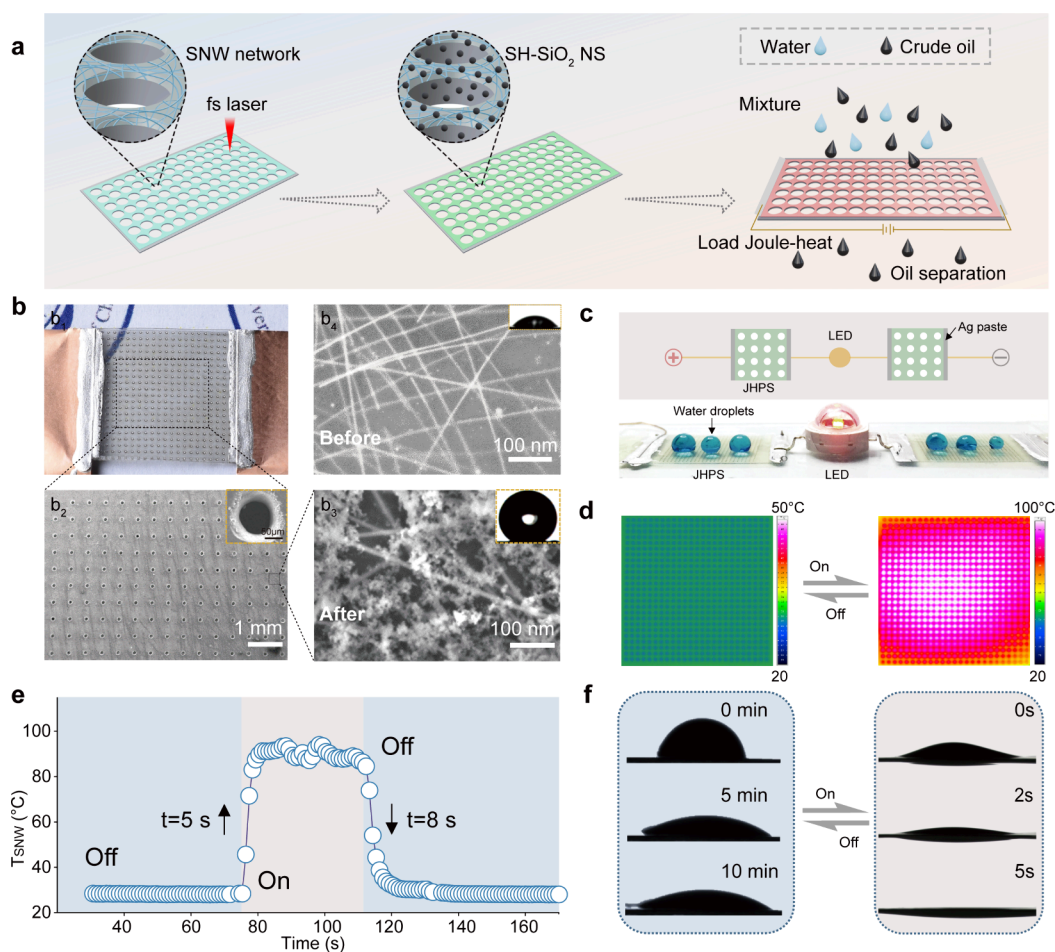


Figure 1. Morphology and electrical characterization of JHPS. (a) Schematic diagram of fabrication. (b) The optical and SEM images of JHPS (b_1 – b_3) and SEM image of porous SNW film without SiO_2 modification (b_4). (c) The photograph of circuit with two JHPS monoliths and a lamp. (d) Comparison of thermal infrared images under the switch off/on. (e) The curve of average temperature vs time under the switch off/on. (f) In situ contact angle measurement of oil droplet under switch-off/on conditions.

skeletons are commercial nano/microporous sponge, which has the limitations of inferior uniformity and poor controllability. As a result, developing a superhydrophobic, energy-efficient, and morphology-controllable separator toward the rapid salvage of heavy crude oil is still a timely need.

To answer the above challenge, we report a Joule-heated hydrophobic porous separator (JHPS) by incorporating a porous silver nanowire film and superhydrophobic SiO_2 nanoparticles (SH- SiO_2 NPs), which has the advantages of low energy consumption ($169.7 \text{ }^\circ\text{C cm}^2 \text{ W}^{-1}$), a short thermal-response time ($\sim 5 \text{ s}$), and a rapid heating rate ($\sim 13 \text{ }^\circ\text{C/s}$).^{26,27} By taking advantage of a femtosecond laser with high peak power density and low thermal-effect, we could rapidly obtain a highly arrayed porous SNW heater as the heavy oil/water separator. Importantly, SiO_2 nanoparticles could be homogeneously decorated on Ag nanowire surface to repel the water phase. When an ultralow voltage (4.5 V) is applied, joule heating decreases the crude oil's viscosity by as much as 3 orders of magnitude, thereby facilitating oil infiltration through the JHPS within 5 s. Significantly, infiltration occurs only from the SNW face to the PI face, and the mechanism of directional infiltration is attributed to the Marangoni-effect-induced gradient wettability. This work provides a new avenue for heavy crude oil/water separation.

Figure 1a shows the preparation process of the Joule-heated hydrophobic porous separator (JHPS). Here, the SNW film is 125- μm -thick PI film coated with 100 nm-thick silver nanowires, and intrinsic resistance is 20–30 Ω . Femtosecond laser (fs laser) is first adopted to process the SNW film to form a through-hole microcone array by circle-scanning method, where the diameter and spacing of the microcone array are adjusted by operating the laser spot. Subsequently, hydrophobic modification is implemented by spraying superhydrophobic SiO_2 nanoparticles onto the SNW face of porous SNW film. The superhydrophobic surface can prevent water infiltrating, while allowing crude oil to infiltrate after heating. The optical image of the JHPS in Figure 1b₁ shows a high transmittance, which indicates that no sediment is deposited on the surface due to the fs laser processing. Figure 1b₂ shows the SEM images of the JHPS. It is clear that the microcone is through-hole, which proves that nanoparticle modification does not block the channel. Furthermore, the morphologies of the silver nanowires before and after SiO_2 modification are compared in Figures 1b₃–b₄. The initial nanowires are smooth, and the diameter is approximately 10 nm. After modification, SiO_2 nanoparticles are uniformly distributed on the surface of the silver nanowires. The insets show the change in the contact angle from 30° to 150° after modification and exhibit the hydrophobic performance of the JHPS. Figure 1c shows an optical image of two pieces of JHPS

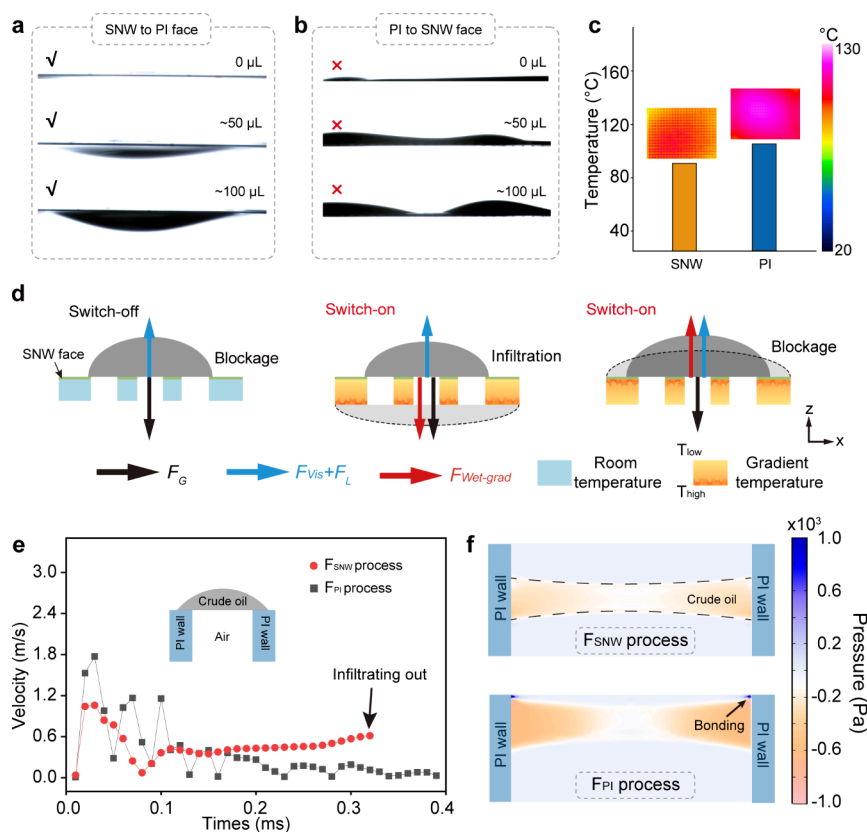


Figure 2. Principle of crude oil infiltration. (a–b) contact angle measurements of oil droplet with the different volumes for F_{SNW} and F_{PI} processes, respectively. (c) Comparison of thermal infrared images of SNW and PI faces. (d) Schematic diagrams of force analysis of crude oil. (e) The velocity-time curve for forward contact line moving. (f) The pressure distribution of oil droplet moving in microcone. Upward direction of force is positive.

connected in series with a LED lamp. The spherical droplets and light LED lamp reveal the hydrophobicity and conductivity of the JHPS. Further, the surface temperature of JHPS before and after hydrophobic modification has almost no attenuation (Figure S1), which indicated that SiO₂ particles modification will not affect the electrical and Joule-heated properties of JHPS. Moreover, the current has almost no attenuation after bending 10 cycles of JHPS (Figure S2), which shows that JHPS has high mechanical properties. Notably, due to the low thermal effect of femtosecond laser processing, the ablated SNW film remains electronic. An infrared image of the JHPS exhibits a uniform distribution of surface temperatures under the switch-on condition, as shown in Figure 1d, and the high-temperature surface is attributed to the Joule-heated effect. Moreover, the average temperature on the SNW face of the JHPS can quickly increase from 23 to 90 °C within 5 s (~13 °C/s of heating rate) and then decrease to room temperature within 8 s, which indicates rapid thermal-response performance (Figure 1e). The infiltration process of the crude oil droplet is recorded by the optical image in Figure 1f. Under the switch-off condition, oil droplet spreads horizontally on the SNW face (upper surface) but does not infiltrate to the PI face (lower surface). When the switch is on, the oil droplet can infiltrate quickly through JHPS within 5 s. As for the water droplet, the contact angle is hardly affected by the voltage (Figure S3), and the infiltration process does not occur on either face under voltage (Figure S4), which proves that JHPS has the selective infiltration of crude oil. The infiltration mechanism of crude oil will be discussed in detail below.

To study the mechanism of infiltration, the oil droplets are placed on the SNW and PI faces of the JHPS, respectively, to compare the infiltration behavior. Two flow processes are named “ F_{SNW} ” and “ F_{PI} ”. For the F_{SNW} process, the oil droplet quickly infiltrates through the JHPS with volumes of 50 and 100 μL (Figure 2a). Conversely, for the F_{PI} process (Figure 2b), a 50 μL oil droplet spreads out only along the PI face of the JHPS. Even when the volume of the oil droplet reaches 100 μL, infiltration still does not occur. This shows that crude oil follows unidirectional infiltration in the JHPS. We monitor the temperature distribution on the SNW and PI faces, as shown in Figure 2c. When the voltage is applied, the average temperature of the SNW face reaches to 90 °C, whereas the temperature of the PI face is 105 °C. Thus, it is speculated that the infiltration behavior of oil droplet is subjected to gradient wettability,^{28–30} caused by the temperature difference between two faces. Figure 2d shows the schematic diagram of the infiltration process and force analysis. The oil droplet is loaded by three main forces including mg (F_G), viscous force (F_{Vis}), and Laplace force (F_L). Under switch-off conditions, crude oil maintains high viscosity, which inhibits the infiltration of oil droplets ($F_{Vis} + F_L$ is larger than F_G). When the switch is on, the Joule-heated effect reduces the viscous resistance of crude oil, which facilitates the infiltration process. Additionally, the gradient wettability caused by the temperature difference creates an extra gradient-wettability force ($F_{Wet-grad}$). For F_{SNW} , increasing temperature along “-z” axis results in better lipophilicity, which generates downward $F_{Wet-grad}$ and drives the oil droplet through the microcone ($F_{Vis} + F_L < F_G + F_{Wet-grad}$). However, for the F_{PI} process, the $F_{Wet-grad}$ points

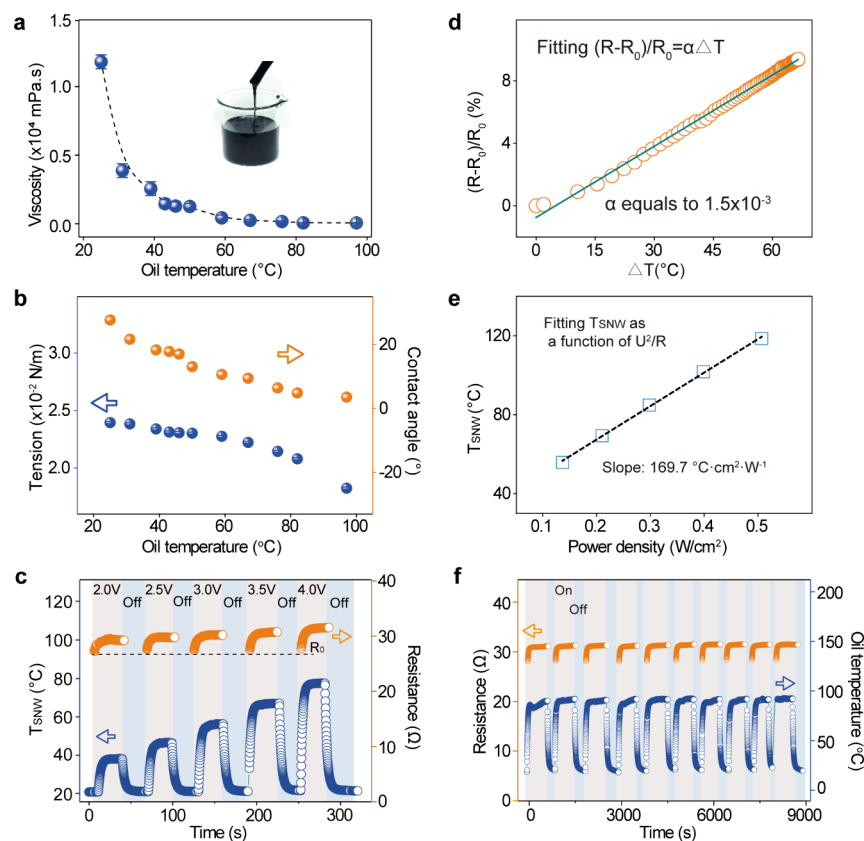


Figure 3. Effect of Joule heating on the crude oil kinetics. (a) The relationship of viscosity and mass density with oil temperature. (b) The relationship of surface tension and contact angle with oil temperature. (c) The temperature and resistance change of JHPS-140 (with a circling diameter of $140 \mu\text{m}$) versus time under multivoltage steps. (d) $(R - R_0)/R_0 - \Delta T$ linear curve. (e) The relationship of temperature with power density. U is the voltage, and R is the resistance. (f) The temperature and resistance change with transition of switch between on and off.

upward ($F_{\text{Vis}} + F_{\text{L}} + F_{\text{Wet-grad}} > F_{\text{G}}$), which prevents the infiltration of an oil droplet. We also simulate the infiltration process of oil droplets in microcone by COMSOL Multiphysics, and the simulation model is shown in the inset of Figure 2e. The motion velocity of forward contact line is monitored. For the F_{SNW} process, the velocity first increases rapidly in a short time, which is attributed to the instantaneous acceleration caused by the rapid deformation of the oil droplet. Then, the velocity decreases and gradually stabilizes, until the droplet ultimately infiltrates out of the microcone. However, for the F_{PI} process, the velocity oscillates obviously and then decreases to zero, which indicates that the oil droplet is bound in the microcone. We further explore the pressure profile of the oil droplet, as shown in Figure 2f. For the F_{PI} process, the oil droplet is subjected to a large upward pressure at the receded contact line, which is considered to be the main cause for inhibiting the infiltration of oil droplet. On the contrary, the droplet gets downward force to accelerate the infiltration in the F_{SNW} process.

The infiltration kinetics of crude oil is determined by the properties of viscosity and surface tension. Effect of joule heat is studied on the properties of the crude oil. Figure 3a shows that the viscosity decreases rapidly with an increasing temperature and then remains stable when the oil temperature exceeds $40 \text{ }^{\circ}\text{C}$. As the major resistance, the low viscosity leads to a small viscous force to enhance infiltration kinetics. Figure 3b shows the curves of the surface tension and contact angle with respect to the oil temperature on the flat SNW film. The surface tension tends to decrease with increasing temperature, and the change in the contact angle is consistent with the surface tension. The good

wettability of the SNW surface is beneficial to the infiltration of crude oil through the microcone. Additionally, the Joule-heated effect of Ag nanowires is the basis of our design for the highly effective crude oil separation. Figure 3c shows the curves of the surface temperature (T_{SNW}) and resistance (R) change at multivoltage steps from 2.0 to 4.0 V. The maximum T_{SNW} and R increase with increasing temperature. In each voltage step, T_{SNW} and R increase sharply to the maximum temperature with the switch on and decrease suddenly to room temperature with the switch off. Two processes of temperature change are completed in 10 s, which shows that the JHPS has a rapid thermal-response performance. Notably, the R_0 (initial resistance) remains unchanged under five voltage steps. This indicates that the SNW does not undergo oxidation at high temperatures, and remains the stability of structure. Figure 3d shows that $(R - R_0)/R_0$ remains positively correlated with ΔT . According to the Resistance–Temperature formula $R = R_0(1 + \alpha \Delta T)$, α (Resistance–Temperature coefficient) is calculated to be 1.5×10^{-3} , and the positive value is consistent with the resistance change in Figure 3c. Besides, the energy consumption is also studied by exploring the relationship between T_{SNW} and power density, as shown in Figure 3e. The slope is calculated to be $169.7 \text{ }^{\circ}\text{C}\cdot\text{cm}^2\cdot\text{W}^{-1}$, which reflects the low energy consumption of the JHPS. Furthermore, the JHPS is repeatedly switched between on and off for 9000 s under 4.5 V (Figure 3f). The unchanged values of R exhibit the high stability of JHPS, and the fast response of oil temperature shows JHPS's excellent heating performance.

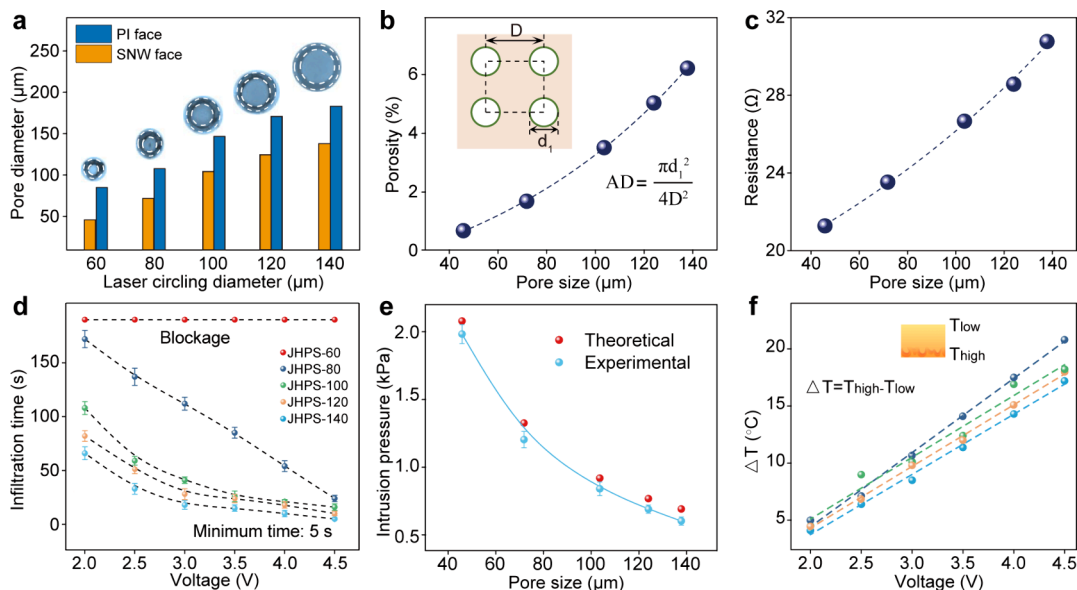


Figure 4. Effect of the circling diameter and the voltage on oil infiltration through JHPS. (a) The relationship of actual diameters of pores on SNW and PI faces with circling diameter. (b) The curve of the porosity of pores on the SNW face with circling diameter. (c) The curve of resistance of JHPS with circling diameter. (d) The curve of penetration time with voltage and circling diameter. (e) The relationship of F_L with the circling diameter. (f) The relationship of temperature difference (ΔT) between two faces with voltage and circling diameter.

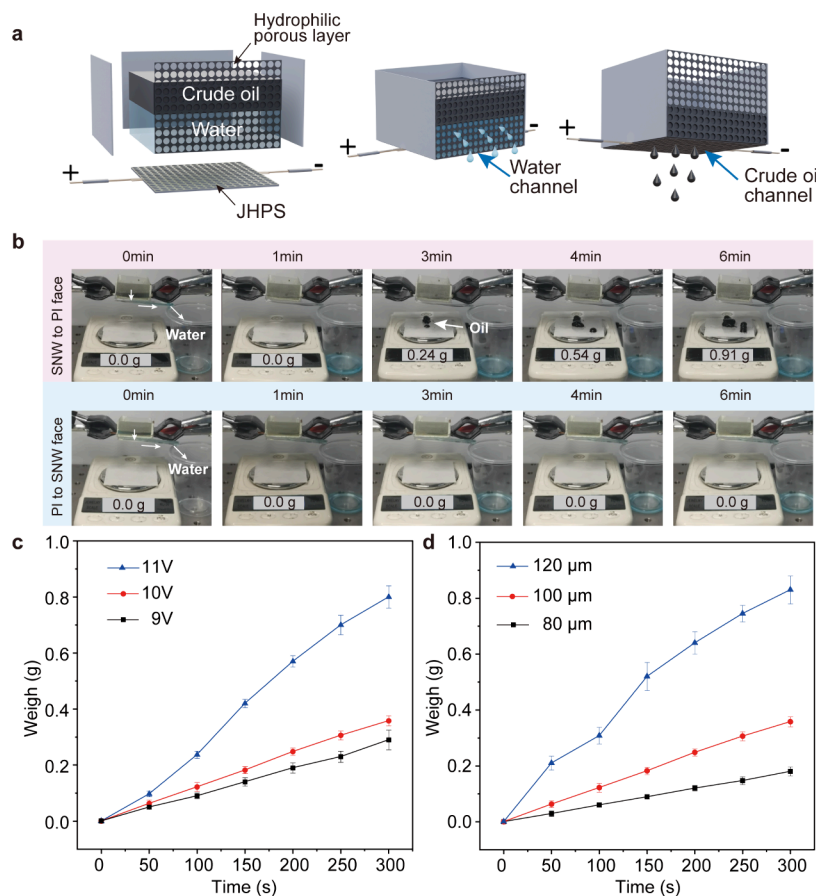


Figure 5. Measurement of crude oil–water separation. (a) The schematic diagram of crude oil–water separation device and separation process. (b) In situ monitoring for continuously collecting the crude oil from the surface of water. (c–d) The relationship of velocity of oil infiltration with pore size and voltage, respectively.

It is well-known that porosity is a crucial factor in infiltration performance. By adjusting the circling diameter, JHPSs with different size of microcone structure are prepared, as shown in

Figure 4a. It can be clearly seen that the diameter of the pore on the PI face is larger than that on the SNW face, which is determined by the shape of focus light. The difference in the

diameters of the two pores are almost constant at 50 μm and independent of the circling diameter. Figure 4b shows the curve of porosity on the SNW face with the circling diameter. When the circling diameter is 140 μm , the porosity reaches 6%. Additionally, R of the JHPS is also controlled by the circling diameter. In Figure 4c, R increases with the circling diameter increasing. Even up to 140 μm , JHPS still remains conductive. However, when the circling diameter increases to 160 μm , the JHPS becomes nonconducting, which reveals that the JHPS must maintain the minimum coverage of SNW to keep conductive. Furthermore, an infiltration experiment of viscous crude oil through JHPS is implemented. Figure 4d shows the curve of infiltration time versus voltage for JHPSs with the different circling diameters, and the infiltration processes are recorded in Figure S5. For JHPS-60 (with a circling diameter of 60 μm), crude oil cannot infiltrate at any voltage from 2.0 to 4.5 V, which indicates that the infiltration occurs with a lower limit of pore size. When the circling diameter is greater than 60 μm , the infiltration velocity positively correlates with the circling diameter. It is considered that Laplace pressure (F_L) is the main reason to control infiltration. The relationship between F_L and the circling diameter determined by the equal pressure difference method is shown in Figure 4e. F_L shows an exponential decreasing tendency with the diameter increasing, which indicates that the pore size has a crucial effect on infiltration velocity. Besides, the applied voltage is also a significant factor for oil's infiltration (Figure 4d). As the voltage increases, the infiltration time first decreases sharply and then remains stable when exceeding 3.5 V. Even when the voltage reaches 4.5 V, 50 μL of crude oil infiltrates through JHPS-140 in only 5 s. These results are attributed to the decreasing viscosity force (F_{vis}) caused by joule heat. Additionally, the temperatures of the two faces at different voltages are shown in Figure S6 and S7. Temperature difference (ΔT) increases linearly with voltage for all of the JHPSs (Figure 4f), and the larger ΔT results in greater $F_{\text{wet-grad}}$ to accelerate oil infiltration.

To separate and collect viscous crude oil in the sea, we designed an oil–water separation device. Figure 5a simulates the extraction of crude oil floated on the water surface. The JHPS is located at the bottom of device with an area of 3 cm \times 3 cm and serves as the oil-flow channel. The side walls of the device are PAN films, in which the front wall is hydrophilic and porous for the water-flow channel. Water first infiltrates through the hydrophilic front wall and then flows along the guide groove. Subsequently, floated crude oil comes into contact with the JHPS, and melts to infiltrate through the JHPS. For the F_{SNW} process (Figure 5b), crude oil quickly infiltrates through the bottom wall and falls on the balance. 0.91 g of crude oil is obtained after 6 min. However, for the F_{PI} process, water infiltrates out of the front wall, whereas heavy crude oil cannot infiltrate through the JHPS. Furthermore, we study the effects of the circling diameter and voltage on the infiltration velocity of crude oil. At 10 V (Figure 5c), the continuous velocities of JHPS-80, JHPS-100, and JHPS-120 are 0.03, 0.08, and 0.18 g/min, respectively, which indicates that the infiltration velocity is positively correlated with the pore size. Figure 5d shows the curve of the velocity with the voltage for the JHPS-100 sample. When voltages of 9, 10, and 11 V are applied, the surface T_{SNW} is 58, 69, and 80 $^{\circ}\text{C}$, respectively. As the voltage increases from 9 to 10 V, the velocity increases from 0.06 to 0.08 g/min. Even up to 11 V, the velocity increases to 0.18 g/min, which is 2.5 times larger than that at 10 V. It indicates that the voltage plays a dominant role in infiltration velocity.

In this work, a Joule-heated hydrophobic porous separator was fabricated by combining a porous SNW film and SiO_2 hydrophobic modification. JHPS exhibits the efficient heating performance of low energy consumption ($169.7\text{ }^{\circ}\text{C}\cdot\text{cm}^2\cdot\text{W}^{-1}$), short thermal response time ($\sim 5\text{ s}$), and a rapid heating rate ($\sim 13\text{ }^{\circ}\text{C}/\text{s}$). Significantly, the unidirectional infiltration exists from SNW face to PI face, which is attributed to the gradient wettability caused by temperature difference. Ultimately, the successful deployment of a self-made device enables continuous separation of viscous oil and water. This work provides a new avenue for heavy oil remedy.

■ ASSOCIATED CONTENT

Data Availability Statement

The data that support the findings of this study are available from the corresponding author upon reasonable request.

Supporting Information

The Supporting Information is available free of charge at <https://pubs.acs.org/doi/10.1021/acs.nanolett.4c05496>.

Methods; Surface temperature of JHPS before and after superhydrophobic SiO_2 modification; Current change of JHPS after bending cycles; Contact angles under the voltage on SNW and PI faces; Variation of contact angles under the voltage on SNW and PI faces; Contact angle measurement of infiltration processes for 50 μL crude oil under the different voltages; Thermal images of two faces of JHPSs under the different voltages; Average temperature measurement of two faces of JHPS for heating stability under the different voltages (PDF)

■ AUTHOR INFORMATION

Corresponding Authors

Chaowei Wang – CAS Key Laboratory of Mechanical Behavior and Design of Materials, Department of Precision Machinery and Precision Instrumentation, University of Science and Technology of China, Hefei, Anhui 230027, China; Email: chaoweiw@ustc.edu.cn

Dong Wu – CAS Key Laboratory of Mechanical Behavior and Design of Materials, Department of Precision Machinery and Precision Instrumentation, University of Science and Technology of China, Hefei, Anhui 230027, China; orcid.org/0000-0003-0623-1515; Email: dongwu@ustc.edu.cn

Authors

Youdi Hu – CAS Key Laboratory of Mechanical Behavior and Design of Materials, Department of Precision Machinery and Precision Instrumentation, University of Science and Technology of China, Hefei, Anhui 230027, China

Chao Chen – Department of Materials Physics and New Energy Device, School of Materials Science and Engineering, Hefei University of Technology, Hefei, Anhui 230009, China; orcid.org/0000-0002-8061-0292

Qing-Fang Guan – Department of Chemistry, Institute of Biomimetic Materials & Chemistry, Anhui Engineering Laboratory of Biomimetic Materials, Division of Nanomaterials & Chemistry, Hefei National Research Center for Physical Sciences at the Microscale, University of Science and Technology of China, Hefei 230026, China; orcid.org/0000-0002-9491-7359

Yanlei Hu – CAS Key Laboratory of Mechanical Behavior and Design of Materials, Department of Precision Machinery and

Precision Instrumentation, University of Science and Technology of China, Hefei, Anhui 230027, China; orcid.org/0000-0003-1964-0043

Jincheng Ni – CAS Key Laboratory of Mechanical Behavior and Design of Materials, Department of Precision Machinery and Precision Instrumentation, University of Science and Technology of China, Hefei, Anhui 230027, China

Shu-Hong Yu – Department of Chemistry, Institute of Biomimetic Materials & Chemistry, Anhui Engineering Laboratory of Biomimetic Materials, Division of Nanomaterials & Chemistry, Hefei National Research Center for Physical Sciences at the Microscale, University of Science and Technology of China, Hefei 230026, China; orcid.org/0000-0003-3732-1011

Complete contact information is available at: <https://pubs.acs.org/10.1021/acs.nanolett.4c05496>

Author Contributions

[†]Y.H. and C.C. contributed equally to this work. S.Y., Y.H., and D.W. conceived and designed the experiment. Y.H., C.C., and C.W. fabricated the samples. Y.H., C.C., and Q.G. performed the measurements. Y.H., J.N., and C.C. analyzed the data. Y.H. and C.W. wrote the manuscript.

Notes

The authors declare no competing financial interest.

ACKNOWLEDGMENTS

This work was financially supported by National Natural Science Foundation of China (Nos. U20A20290, 52005475, 52305319, 52105492, 62475252) and Natural Science Foundation of Anhui Province (No. JZ2024AKZR0561). SEM characteristic in this work were carried out at the USTC Center for Micro- and Nanoscale Research and Fabrication. Raman spectra were carried out at Instruments Center for Physical Science, University of Science and Technology of China.

REFERENCES

- (1) Ge, J.; Wang, F.; Yin, X.; Yu, J.; Ding, B. Polybenzoxazine-Functionalized Melamine Sponges with Enhanced Selective Capillarity for Efficient Oil Spill Cleanup. *ACS Appl. Mater. Interfaces* **2018**, *10* (46), 40274–40285.
- (2) Chu, Z.; Feng, Y.; Seeger, S. Oil/Water Separation with Selective Superantwettable/Superwetting Surface Materials. *Angew. Chem., Int. Ed.* **2015**, *54* (8), 2328–2338.
- (3) Li, S.; Dong, R.; Musteata, V.-E.; Kim, J.; Rangnekar, N. D.; Johnson, J. R.; Marshall, B. D.; Chisca, S.; Xu, J.; Hoy, S.; McCool, B. A.; Nunes, S. P.; Jiang, Z.; Livingston, A. G. Hydrophobic polyamide nanofilms provide rapid transport for crude oil separation. *Science* **2022**, *377*, 1555–1561.
- (4) Yang, X.; Sun, P.; Wen, Y.; Mane, A. U.; Elam, J. W.; Ma, J.; Liu, S.; Darling, S. B.; Shao, L. Protein-activated atomic layer deposition for robust crude-oil-repellent hierarchical nano-armored membranes. *Sci. Bull.* **2024**, *69* (2), 218–226.
- (5) Yan, K.; Zhao, F.; Pan, L.; Jiang, Y.; Shi, Y.; Yu, G. High-throughput clean-up of viscous oil spills enabled by a gel-coated mesh filter. *Nat. Sustain.* **2023**, *6* (12), 1654–1662.
- (6) Xiang, B.; Liu, Q.; Yan, W.; Wei, Y.; Mu, P.; Li, J. Advances in special wetttable materials for adsorption separation of high-viscosity crude oil/water mixtures. *Chem. Commun.* **2023**, *59* (49), 7559–7578.
- (7) Huang, W.; Zhang, L.; Lai, X.; Li, H.; Zeng, X. Highly hydrophobic F-rGO@wood sponge for efficient clean-up of viscous crude oil. *Chem. Eng. J.* **2020**, *386* (1), 123994.
- (8) Yuan, J.; Zhang, M.; Xia, M.; Cao, W.; Du, M.; Dou, J.; Zhao, D. Novel high-capacity and reusable carbonaceous sponges for efficient absorption and recovery of oil from water. *Appl. Surf. Sci.* **2019**, *487* (1), 398–408.
- (9) Lv, X.; Tian, D.; Peng, Y.; Li, J.; Jiang, G. Superhydrophobic magnetic reduced graphene oxide-decorated foam for efficient and repeatable oil-water separation. *Appl. Surf. Sci.* **2019**, *466* (1), 937–945.
- (10) Luo, Z.; Wang, X.; Yang, D.; Zhang, S.; Zhao, T.; Qin, L.; Yu, Z.-Z. Photothermal hierarchical carbon nanotube/reduced graphene oxide microspherical aerogels with radially orientated microchannels for efficient cleanup of crude oil spills. *J. Colloid Interface Sci.* **2020**, *570* (1), 61–71.
- (11) Chang, J.; Shi, Y.; Wu, M.; Li, R.; Shi, L.; Jin, Y.; Qing, W.; Tang, C.; Wang, P. Solar-assisted fast cleanup of heavy oil spills using a photothermal sponge. *J. Mater. Chem. A* **2018**, *6* (19), 9192–9199.
- (12) Liu, Y.; Su, Y.; Guan, J.; Cao, J.; Zhang, R.; He, M.; Gao, K.; Zhou, L.; Jiang, Z. 2D Heterostructure Membranes with Sunlight-Driven Self-Cleaning Ability for Highly Efficient Oil-Water Separation. *Adv. Funct. Mater.* **2018**, *28* (13), 1706545.
- (13) Sheng, W.; Li, W.; Yu, B.; Li, B.; Jordan, R.; Jia, X.; Zhou, F. Mussel-Inspired Two-Dimensional Freestanding Alkyl-Polydopamine Janus Nanosheets. *Angew. Chem., Int. Ed.* **2019**, *58* (35), 12018–12022.
- (14) Liu, Y.; Li, W.; Yuan, C.; Jia, L.; Liu, Y.; Huang, A.; Cui, Y. Two-Dimensional Fluorinated Covalent Organic Frameworks with Tunable Hydrophobicity for Ultrafast Oil-Water Separation. *Angew. Chem., Int. Ed.* **2022**, *61* (2), No. e202113348.
- (15) Ge, J.; Shi, L.-A.; Wang, Y.-C.; Zhao, H.-Y.; Yao, H.-B.; Zhu, Y.-B.; Zhang, Y.; Zhu, H.-W.; Wu, H.-A.; Yu, S.-H. Joule-heated graphene-wrapped sponge enables fast clean-up of viscous crude-oil spill. *Nat. Nanotechnol.* **2017**, *12* (5), 434–440.
- (16) Hao, W.; Xu, J.; Li, R.; Zhao, X.; Qiu, L.; Yang, W. Developing superhydrophobic rock wool for high-viscosity oil/water separation. *Chem. Eng. J.* **2019**, *368* (1), 837–846.
- (17) Shi, L.-A.; Ge, J.; Hu, B.-C.; Ma, T.; Zhao, H.; Song, Y.-H.; Li, C.; Yu, S.-H. Joule-heated carbonized melamine sponge for high-speed absorption of viscous oil spills. *Nano Res.* **2021**, *14* (8), 2697–2702.
- (18) Zhang, C.; Wu, M.-B.; Wu, B.-H.; Yang, J.; Xu, Z.-K. Solar-driven self-heating sponges for highly efficient crude oil spill remediation. *J. Mater. Chem. A* **2018**, *6* (19), 8880–8885.
- (19) Li, Q.; Sun, Q.; Li, Y.; Wu, T.; Li, S.; Zhang, H.; Huang, F. Solar-Heating Crassula perforata-Structured Superoleophilic CuO@CuS/PDMS Nanowire Arrays on Copper Foam for Fast Remediation of Viscous Crude Oil Spill. *ACS Appl. Mater. Interfaces* **2020**, *12* (17), 19476–19482.
- (20) Kuang, Y.; Chen, C.; Chen, G.; Pei, Y.; Pastel, G.; Jia, C.; Song, J.; Mi, R.; Yang, B.; Das, S.; Hu, L. Bioinspired Solar-Heated Carbon Absorbent for Efficient Cleanup of Highly Viscous Crude Oil. *Adv. Funct. Mater.* **2019**, *29* (16), 1900162.
- (21) Chao, W.; Wang, S.; Li, Y.; Cao, G.; Zhao, Y.; Sun, X.; Wang, C.; Ho, S.-H. Natural sponge-like wood-derived aerogel for solar-assisted adsorption and recovery of high-viscosity crude oil. *Chem. Eng. J.* **2020**, *400* (1), 125865.
- (22) Sun, A.; Hou, X.; Hu, X. Super-performance photothermal conversion of 3D macrostructure graphene-CuFeSe₂ aerogel contributes to durable and fast clean-up of highly viscous crude oil in seawater. *Nano Energy* **2020**, *70* (1), 104511.
- (23) Qi, L.; Zhiheng, W.; Yimin, D.; Ling, C.; Chengqian, F.; Shengyun, W.; Yue-fei, Z.; Yan, L.; Li, W. Preparation of novel magnetic hydrophobic and lipophilic polyurethane sponge for effective separation of oil/water mixtures. *J. Mater. Sci. Mater. Electron* **2021**, *32* (22), 26291–26305.
- (24) Latthe, S. S.; Sutar, R. S.; Shinde, T. B.; Pawar, S. B.; Khot, T. M.; Bhosale, A. K.; Sadasivuni, K. K.; Xing, R.; Mao, L.; Liu, S. Superhydrophobic Leaf Mesh Decorated with SiO₂ Nanoparticle-Polystyrene Nanocomposite for Oil-Water Separation. *ACS Appl. Nano Mater.* **2019**, *2* (2), 799–805.
- (25) Oribayo, O.; Feng, X.; Rempel, G. L.; Pan, Q. Synthesis of lignin-based polyurethane/graphene oxide foam and its application as an absorbent for oil spill clean-ups and recovery. *Chem. Eng. J.* **2017**, *323* (1), 191–202.

(26) Chen, C.; Huang, Z.; Jiao, Y.; Shi, L.-A.; Zhang, Y.; Li, J.; Li, C.; Lv, X.; Wu, S.; Hu, Y.; Zhu, W.; Wu, D.; Chu, J.; Jiang, L. In Situ Reversible Control between Sliding and Pinning for Diverse Liquids under Ultra-Low Voltage. *ACS Nano* **2019**, *13* (5), 5742–5752.

(27) Chen, C.; Huang, Z.; Zhu, S.; Liu, B.; Li, J.; Hu, Y.; Wu, D.; Chu, J. In Situ Electric-Induced Switchable Transparency and Wettability on Laser-Ablated Bioinspired Paraffin-Impregnated Slippery Surfaces. *Adv. Sci.* **2021**, *8* (14), 2100701.

(28) Ren, F.; Li, G.; Zhang, Z.; Zhang, X.; Fan, H.; Zhou, C.; Wang, Y.; Zhang, Y.; Wang, C.; Mu, K.; Su, Y.; Wu, D. A single-layer Janus membrane with dual gradient conical micropore arrays for self-driving fog collection. *J. Mater. Chem. A* **2017**, *5* (35), 18403–18408.

(29) Hu, Y.; Qiu, W.; Zhang, Y.; Zhang, Y.; Li, C.; Li, J.; Wu, S.; Zhu, W.; Wu, D.; Chu, J. Channel-controlled Janus membrane fabricated by simultaneous laser ablation and nanoparticles deposition for underwater bubbles manipulation. *Appl. Phys. Lett.* **2019**, *114* (17), 173701.

(30) Zhu, S.; Li, J.; Cai, S.; Bian, Y.; Chen, C.; Xu, B.; Su, Y.; Hu, Y.; Wu, D.; Chu, J. Unidirectional Transport and Effective Collection of Underwater CO₂ Bubbles Utilizing Ultrafast-Laser-Ablated Janus Foam. *ACS Appl. Mater. Interfaces* **2020**, *12* (15), 18110–18115.